starting to become significant on the exchange broadening time scale at 369 K, although the experimental data are insufficient to demonstrate this conclusively. The separation between the resonance of the η-C_5H_5 carbon atoms and the shoulder to low field, which could perhaps be the averaged resonance for the σ-C_5H_5 carbon atoms, is approximately 70 Hz. This compares to a 75-Hz separation between the resonances of the σ- and η-cyclopentadienyl protons in the 100-MHz NMR spectrum in toluene at 240 K.[24] Since in solution the ligand functionality interchange reaches the fast limit on the exchange broadening time scale above about 330 K, this implies that the ring-interchange process is significantly slowed in the crystalline state in comparison to in solution.

Conclusions

The ^{13}C CP/MAS NMR spectrum of **1** indicates that the rate of sigmatropic rearrangement of the σ-C_5H_5 ring is significant on the NMR time scale at temperatures above 180 K. This rearrangement could be followed through the exchange broadening, MAS broadening, and dipolar broadening regimes. Magnetization-transfer experiments in the slow exchange limit are consistent with [1,2] sigmatropic shifts being the dominant rearrangement mechanism, although interestingly some contribution from [1,3] shifts is indicated by the data. Exchange rates for this rearrangement process, calculated from fitting of the exchange-broadened line shapes to those expected for a [1,2] shift process, follow an Arrhenius relation with activation energy E_a = 33.2 ± 1.0 kJ mol^{-1} and frequency factor $A = 2.9 \times 10^{10}$ s^{-1}. This rearrangement, therefore, appears to occur with similar facility in the solid state and in solution, suggesting that the activation energy for this process is determined principally by electronic factors, which are expected to be similar in the two states. By contrast, the ring-interchange process appears substantially retarded in the crystalline state as compared with that in the solution state. This indicates that the activation energy for this motion, which involves substantial rearrangement of atoms and disruption to the molecular packing, is significantly increased by the intermolecular interactions present in the crystalline state.

Acknowledgment. We are grateful to Drs. N. J. Clayden, J. M. Twyman, G. Stringer, and A. Sella for expert assistance and advice. We thank the SERC for financial assistance.

Solid-State ^{199}Hg and ^{113}Cd NMR Studies of Mercury- and Cadmium-Thiolate Complexes. Spectroscopic Models for [Hg(SCys)$_n$] Centers in the Bacterial Mercury Resistance Proteins

Rodolfo A. Santos, Eric S. Gruff, Stephen A. Koch,* and Gerard S. Harbison*

Contribution from the Department of Chemistry, State University of New York at Stony Brook, Stony Brook, New York 11794-3400. *Received June 7, 1990*

Abstract: ^{199}Hg CP/MAS-NMR spectra have been measured for representative examples of the major coordination geometries available to monomeric mercury thiolate complexes: $[Hg(SR)_2]$, $[Hg(SR)_3]^{1-}$, and $[Hg(SR)_4]^{2-}$. Solid-state ^{113}Cd NMR spectra have been measured for related $[Cd(SR)_3]^{1-}$ compounds. $[(n\text{-}Bu)_4N][Cd(S\text{-}2,4,6\text{-}i\text{-}Pr_3C_6H_2)_3]$ and $[Ph_4P][Hg(S\text{-}2,3,5,6\text{-}Me_4C_6H)_3]$ were structurally characterized by X-ray crystallography. The metal ions in both compounds are three-coordinate with distorted Y-shaped, planar $[MS_3]$ units. These structures are discussed in relationship to a second conformational isomer, the symmetric C_{3h} $[M(SR)_3]^{1-}$ anion. The shielding tensor, isotropic chemical shift (σ_{iso}), the chemical shielding anistropy ($\Delta\sigma$), and the asymmetry parameter (η) vary in a systematic manner as a function of coordination number and coordination geometry. ^{199}Hg and ^{113}Cd CP/MAS-NMR data for selected compounds (σ_{iso}, $\Delta\sigma$, η) are as follows: $[Hg(S\text{-}2,4,6\text{-}i\text{-}Pr_3C_6H_2)_2]$ (-1015, 4256, 0.16); $[Ph_4P][Hg(S\text{-}2,4,6\text{-}i\text{-}Pr_3C_6H_2)_3]$ (-267, 1408, 0.30), $[(n\text{-}Bu)_4N][Hg(SPh)_3]$ (-341, 1273, 0.97), $[Et_4N]_2[Hg(S\text{-}2\text{-}PhC_6H_4)_4]$ (-433, 86.5, 0.86), and $[Ph_4P][Cd(S\text{-}2,4,6\text{-}i\text{-}Pr_3C_6H_2)_3]$ (668, 483, 0.24). The implications of this study to solution and solid-state ^{199}Hg and ^{113}Cd NMR studies of Hg- and Cd-cysteine proteins are discussed.

The proteins which are involved in bacterial mercury resistance are encoded in a single operon which is regulated under the control of a mercury-sensing DNA-binding protein (MerR).[1] The mer gene encodes a series of proteins which detoxify organomercurials (organomercury lyase) and inorganic mercuric salts (mercuric reductase) by enzymatic conversion to Hg metal. The study of these proteins has stimulated interest in structural and spectroscopic probes which might be used to determine the nature of the coordination of the Hg^{2+} ion to the proteins. Among such probes is ^{199}Hg NMR. As has been shown in numerous studies, NMR is uniquely sensitive to the coordination and environment of metal ions bound to proteins. Thus ^{113}Cd has been used to probe the nature of metal binding in metallothionein, liver alcohol dehydrogenase, and most recently in the DNA-binding proteins gene 32 and GAL4.[2-7] Given the success of such studies, it is reasonable to consider whether ^{199}Hg, an isotope with a somewhat lower gyromagnetic ratio and natural abundance, but nonetheless favorable compared with, say ^{13}C, might similarly be used to probe mercury binding proteins. The feasibility of such studies hinges critically on the size of the chemical shielding tensor of mercury in typical protein coordination sites. In solution NMR of heavy metals, the chemical shielding tensor is usually the dominant mode

(1) Walsh, C. T.; Distefano, M. D.; Moore, M. J.; Shewchuk, L. M.; Verdine, G. L. *FASEB J.* **1988**, *2*, 124. O'Halloran, T. V. *Met. Ions Biol. Sys.* **1989**, *25*, 105. Brown, N. L. *Trends Biochem. Sci.* **1985**, *10*, 400. Silver, S.; Misra, T. K. *Ann. Rev. Microbiol.* **1988**, *42*, 717.

(2) Summers, M. F. *Coord. Chem. Rev.* **1988**, *86*, 43.

(3) Otvos, J. D.; Olafson, R. W.; Armitage, I. M. *J. Biol. Chem.* **1982**, *257*, 2427.

(4) Bobsein, B. R.; Myers, R. J. *J. Am. Chem. Soc.* **1980**, *102*, 2454. Bobsein, B. R.; Myers, R. J. *J. Biol. Chem.* **1981**, *256*, 5313.

(5) Giedroc, D. P.; Johnson, B. A.; Armitage, I. M.; Coleman, J. E. *Biochemistry* **1989**, *28*, 2410.

(6) Pan, T.; Coleman, J. E. *Biochemistry* **1990**, *29*, 3023.

(7) Nettesheim, D. G.; Engeseth, H. R.; Otvos, J. D. *Biochemistry* **1985**, *24*, 6744. South, T. L.; Kim, B.; Summers, M. F. *J. Am. Chem. Soc.* **1989**, *111*, 395.

0002-7863/91/1513-469$02.50/0

of relaxation; large CSAs will tend to decrease the T_2 and render NMR signals of proteins of even moderate molecular weight proteins unobservably broad. In solid-state NMR, the CSA does not generally contribute to relaxation, but large shielding tensors similarly disperse the NMR signal over a wide spectral range, worsening the signal-to-noise. Unfortuantely there has been until now very little data regarding the chemical shielding tensors of mercury compounds. Studies using liquid crystal solvents have set the CSA of dimethylmercury at around 7000 ppm,[8] while monoalkylmercury halides have smaller anisotropies on the order of 5000 ppm.[9] Mercuric acetate, in which the mercury ion is in approximately linear coordination between two oxygens, has a CSA of 1700 ppm,[10] while the mercurous ion in mercurous nitrate monohydrate, the only mercury compound studied so far by single crystal solid-state NMR and for which a full shielding tensor has been determined, has a CSA of approximately 3000 ppm.[11] None of these compounds is particularly appropriate for mercury coordination to the mercury resistance proteins since expectations based on the known affinities of mercury, results of molecular biological studies and EXAFS experiments, suggest coordination to sulfur via cysteine side chains.[12-15]

To remedy these deficiencies, we have carried out solid-state ^{199}Hg NMR studies of Hg–thiolate complexes which span the major coordination geometries available to mercury: $[Hg(SR)_2]$, $[Hg(SR)_3]^{1-}$, and $[Hg(SR)_4]^{2-}$. These studies give a general picture of the problems which can be anticipated for ^{199}Hg NMR studies in proteins. We compare these data with spectra of ^{113}Cd in similar or in some cases isomorphous complexes and obtain a general relationship between the shielding tensors of homologous cadmium and mercury species.

Three-coordinate $[Hg(SR)_3]^{1-}$ compounds are of particular interest, since, as we anticipated,[16] Hg^{2+} appears to bind to MerR with a trigonal $[Hg(S\text{–}Cys)_3]$ coordination.[12a,15] On the basis of the structural similarity of Cd– and Hg–thiolate complexes, we have also predicted a three-coordinate $[Cd(SCys)_3]$ center for cadmium bound to the MerR protein. While this manuscript was in preparation, the solid-state ^{199}Hg NMR spectra of a series of Hg–thiolate complexes were reported by Natan et al.[17] However the present results are not in agreement with the latter work.

Experimental Section

Preparation of Compounds. **$[Ph_4P][Cd(S\text{-}2,4,6\text{-}i\text{-}Pr_3C_6H_2)_3]$ (1).**[18] LiS-2,4,6-*i*-$Pr_3C_6H_2$ (1.13 g, 4.66 mmol), $CdCl_2$ (0.18 g, 0.98 mmol), and Ph_4PBr (0.80 g, 1.91 mmol) were combined in a mixture of 5 mL of DMF and 50 mL of *i*-PrOH, and the pale yellow mixture was stirred for 2 h. The mixture was then cooled to −20 °C overnight, and the resultant crystalline white solid was filtered, washed with *i*-PrOH, and dried: yield 0.50 g (45%); ^{1}H NMR ($CDCl_3$) 1.00 ppm (d, 36 H, *o*-CH_3), 1.13 (d, 18 H, *p*-CH_3), 2.72 (m, 3 H, *p*-CH), 4.09 (m, 6 H, *o*-CH), 6.67 (s, 6 H, *m*-H), 7.4–8.0 (m, 20 H, Ph_4P).

$[(n\text{-}Bu)_4N][Cd(S\text{-}2,4,6\text{-}i\text{-}Pr_3C_6H_2)_3]$ (2) was synthesized in a similar manner in 53% yield.

$[(n\text{-}Pr)_4N][Cd(S\text{-}2,4,6\text{-}t\text{-}Bu_3C_6H_2)_3]$. LiS-2,4,6-*t*-$Bu_3C_6H_2$ (0.50 g, 1.8 mmol), $CdCl_2$ (0.10 g, 0.54 mmol), and (*n*-Pr)$_4$NBr (0.15 g, 0.56 mmol) were stirred in 30 mL of CH_3CN for 30 min and filtered *i*-PrOH (50 mL) and 30 mL of water were added to the filtrate to give 0.34 g of product (55% yield).

$[(n\text{-}Pr)_4N][Hg(S\text{-}2,4,6\text{-}i\text{-}Pr_3C_6H_2)_3]$ (3). LiS-2,4,6-*i*-$Pr_3C_6H_2$ (1.04 g, 4.29 mmol), $HgCl_2$ (0.20 g, 0.74 mmol), and (*n*-Pr)$_4$NBr (0.30 g, 1.13 mmol) were combined in 30 mL of CH_3OH, and the mixture stirred for 15 min and then cooled to −20 °C. The following day crystalline pale yellow solid had precipitated from the solution and was collected by vacuum filtration and dried. The yield was 0.58 g (87%): ^{1}H NMR ($CDCl_3$) 0.82 ppm (t, 12 H) $(CH_3CH_2CH_2)_4N$), 1.49 (qt, 8 H), 2.92 (qt, 8 H), 0.93 (d, 36 H, *o*-CH_3), 1.10 (d, 18 H, *p*-CH_3), 2.68 (m, 3 H, *p*-CH), 4.04 (m, 6 H, *o*-CH), 6.67 (s, 6 H, *m*-H).

$[Ph_4P][Hg(S\text{-}2,4,6\text{-}i\text{-}Pr_3C_6H_2)_3]$ (4) was synthesized in 55% yield by using 0.40 g (0.95 mmol) of Ph_4PBr.

$[(n\text{-}Pr)_4N][Hg(S\text{-}2,3,5,6\text{-}Me_4C_6H)_3]$. $HgCl_2$ (0.20 g, 0.74 mmol), LiS-2,3,5,6-Me_4C_6H (1.04 g, 6.04 mmol), and (*n*-Pr)$_4$NBr (0.23 g, 0.86 mmol) were combined in 40 mL of CH_3CN, and the mixture was stirred for 1 h. The clear, colorless solution was cooled to −20 °C for 48 h, resulting in precipitation of colorless, crystalline solid which was filtered, washed with ether, and dried: yield 0.56 g (87%). Attempts to synthesize this product in methanol led to the formation of insoluble white products: ^{1}H NMR ($CDCl_3$) 0.85 ppm (t, 12 H, $(CH_3CH_2CH_2)_4N$), 1.47 (qt, 8 H), 2.91 (tq, 8 H), 2.07, 2.29 (2 s, 2 (18 H), *o,m*-CH_3), 6.39 (s, 4 H, *m*-H).

$[Ph_4P][Hg(S\text{-}2,3,5,6\text{-}Me_4C_6H)_3]$ (5) was synthesized in an identical fashion by using 0.73 g (1.74 mmol) of Ph_4PBr. Yield of **5** was 0.66 g (37%).

$[Hg(S\text{-}2,4,6\text{-}i\text{-}Pr_3C_6H_2)_2]$ (7). Mercuric chloride (0.32 g, 1.18 mmol) was added to an acetonitrile solution of LiS-2,4,6-*i*-$Pr_3C_6H_2$ (0.52 g, 2.15 mmol), and a colorless crystalline solid precipitated after approximately 30 s. The solid was filtered, washed with CH_3CN, and dried. A second crop precipitated from the filtrate after cooling to −20 °C overnight: total yield 0.33 g (47%); ^{1}H NMR ($CDCl_3$) 1.08 ppm (d, 24 H, *o*-CH_3), 1.20 (d, 12 H, *p*-CH_3), 2.80 (m, 2 H, *p*-CH), 3.94 (m, 4 H, *o*-CH), 6.89 (s, 4 H, *m*-H).

X-ray Crystallography. **$[(n\text{-}Bu)_4N][Cd(S\text{-}2,4,6\text{-}i\text{-}Pr_3C_6H_2)_3]$ (2).** Crystals were grown from a slowly cooled methanol solution, and a suitable crystal (0.4 × 0.2 × 0.3 mm) was mounted in a capillary filled with mineral oil. The unit cell was determined to be primitive monoclinic with space group $P2_1/a$ (no. 14). Data were collected from $0° < 2\theta < 46°$, and 3847 unique reflections with $I > 3\sigma(I)$ (of a total of 10027) were used to solve the structure. The cadmium atom was located on a Patterson map, and other non-hydrogen atoms were located on subsequent difference maps. Two of the three thiolate ligands exhibited disordered *p*-isopropyl groups which were successfully modelled. The hydrogen atom positions were calculated, and the non-hydrogen atoms were refined anisotropically, resulting in a final R value of 0.045 and R_w of 0.056. Data collection parameters are listed in Table I. Bond distances and angles are listed in Table II.

Table I. Crystallographic Parameters

	$[(n\text{-}Bu)_4N][Cd(S\text{-}2,4,6\text{-}i\text{-}Pr_3C_6H_2)_3]$ (2)	$[Ph_4P][Hg(S\text{-}2,3,5,6\text{-}Me_4C_6H)_3]$ (5)
formula	$CdS_3NC_{61}H_{105}$	$HgS_3PNC_{56}H_{62}$
formula weight	1061.1	1076.9
a, Å	11.534 (8)	12.907 (3)
b, Å	27.13 (2)	22.155 (5)
c, Å	21.69 (2)	9.443 (8)
α, deg	90	98.35 (5)
β, deg	102.84 (6)	95.48 (4)
γ, deg	90	104.54 (2)
V, Å^3	6619 (17)	2561 (4)
Z	4	2
space group	$P2_1/a$ (no. 14)	$P\bar{1}$ (no. 2)
radiation	Mo Kα (λ = 0.71069)	Mo Kα (λ = 0.71069)
lin abs coeff, cm^{-1}	4.54	31.86
scan mode	$\theta/2\theta$	$\theta/2\theta$
2θ max deg	46.1	50
no. obsvns ($I > 3\sigma(I)$)	3846	6173
no. variables	577	559
R	0.059	0.033
R_w	0.077	0.041

Table II. Selected Bond Distances (Å) and Angles (deg) for $[(n\text{-}Bu)_4N][Cd(S\text{-}2,4,6\text{-}i\text{-}Pr_3C_6H_2)_3]$ (2)

Cd–S1	2.422 (4)	S1–Cd–S2	135.3 (1)	Cd–S1–C11	105.0 (4)
Cd–S2	2.425 (4)	S1–Cd–S3	123.9 (1)	Cd–S2–C21	113.5 (4)
Cd–S3	2.455 (4)	S2–Cd–S3	100.8 (1)	Cd–S3–C31	109.8 (4)

(8) Pulkkinen, A.; Hiltunen, Y.; Jokisaari, J. *Liquid Cryst.* **1988**, *3*, 737. Jokisaari, J.; Diehl, P. *Org. Magn. Reson.* **1980**, *13*, 359.
(9) Kennedy, J. D.; McFarlane, W. *J. Chem. Soc., Faraday Trans. II* **1976**, *72*, 1653.
(10) Harris, R. K.; Sebald, A. *Magn. Reson. Chem.* **1987**, *25*, 1058.
(11) Santos, R. A.; Harbison, G. S. Manuscript in preparation.
(12) (a) Helmann, J. D.; Ballard, B. T.; Walsh, C. T. *Science* **1990**, *247*, 946. (b) Shewchuk, L. M.; Verdine, G. L.; Nash, H.; Walsh, C. T. *Biochemistry* **1989**, *28*, 6140. (c) Shewchuk, L. M.; Verdine, G. L.; Walsh, C. T. *Biochemistry* **1989**, *28*, 2331.
(13) Raybuck, S. A.; Distefano, M. D.; Teo, B.-K.; Orme-Johnson, W.; Walsh, C. T. *J. Am. Chem. Soc.* **1990**, *112*, 1983.
(14) Ralston, D. M.; O'Halloran, T. V. *Proc. Natl. Acad. Sci. U.S.A.* **1990**, *87*, 3846. O'Halloran, T. V.; Frantz, B.; Shin, M. K.; Ralston, D. M.; Wright, J. G. *Cell* **1989**, *56*, 119.
(15) Wright, J. G.; Tsang, H.-T.; Penner-Hahn, J. E.; O'Halloran, T. V. *J. Am. Chem. Soc.* **1990**, *112*, 2434.
(16) Gruff, E. S.; Koch, S. A. *J. Am. Chem. Soc.* **1990**, *112*, 1245.
(17) Natan, M. J.; Millikan, C. F.; Wright, J. G.; O'Halloran, T. V. *J. Am. Chem. Soc.* **1990**, *112*, 3255.
(18) Abbreviations: S-2,4,6-*i*-$Pr_3C_6H_2$ = 2,4,6-triisopropylbenzenethiolate; S-2,3,5,6-Me_4C_6H = 2,3,5,6-tetramethylbenzenethiolate; S-2,4,6-*t*-$Bu_3C_6H_2$ = 2,4,6-tri-*tert*-butylbenzenethiolate; *S*-2PhC_6H_4 = 2-phenylbenzenethiolate.

Table III. Selected Bond Distances (Å) and Angles (deg) for $[Ph_4P][Hg(S\text{-}2,3,5,6\text{-}Me_4C_6H)_3]$ (**5**)

Hg–S1	2.494 (2)	S1–Hg–S2	112.94 (4)	Hg–S1–C11	105.0 (2)
Hg–S2	2.397 (2)	S1–Hg–S3	112.45 (6)	Hg–S2–C21	104.0 (2)
Hg–S3	2.404 (2)	S2–Hg–S3	134.60 (6)	Hg–S3–C31	105.4 (2)

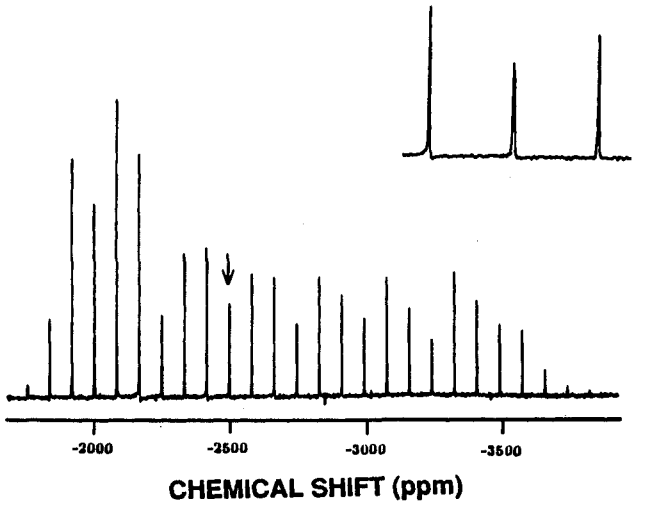

Figure 1. ^{199}Hg CP/MAS NMR spectrum of $Hg(OAc)_2$ at ν_R of 4.4 KHz.

$[Ph_4P][Hg(S\text{-}2,4,6\text{-}i\text{-}Pr_3C_6H_2)_3]$ (4). Colorless crystals were grown from the filtrate of the reaction mixture to which additional *i*-PrOH had been added. The unit cell indicated that it is isomorphous and presumably isostructural with the Cd analogue (**1**). Cell parameters were determined to be a = 15.46 (3) Å, b = 21.28 (3) Å, c = 13.49 (1) Å, α = 94.98 (9)°, β = 114.55 (14)°, γ = 104.51 (14)°, V = 3815 (11) Å^3; and Z = 2. Due to decay of the crystal (presumably due to loss of solvent), no structure determination was possible.

$[Ph_4P][Hg(S\text{-}2,3,5,6\text{-}Me_4C_6H)_3]$ (5). Crystals were grown from a slowly cooled acetonitrile solution (–20 °C). A crystal measuring 0.5 × 0.4 × 0.3 mm was mounted in a capillary, covered with mineral oil, and sealed with epoxy. A unit cell was obtained and determined to be primitive triclinic, space group $P\bar{1}$ (no. 2). A data set was collected from $0° < 2\theta \leq 50°$, resulting in a total of 8955 reflections. After reduction of the data set (6173 reflections with $I > 3\sigma(I)$), the mercury atom was located on a Patterson map, and the remaining non-hydrogen atoms were located on subsequent difference maps. A correction was made for absorption (DIFABS), and hydrogens from methyl groups were located where possible and the rest were calculated (C–H = 0.95 Å). Full anisotropic refinement resulted in final values of R (R_w) = 0.033 (0.045). Data collection parameters are listed in Table I. Bond distances and angles are in Table III.

Solid-State NMR. Both acquisition and analysis of magic angle spinning spectra from samples with large shielding anisotropies require considerable care; neglecting any one of several important factors will introduce severe errors into the determination of the shielding tensor, usually leading to an underestimation of the anisotropy.

As a setup standard and primary reference, we have used mercuric acetate, a sample previously studied by Harris.[10] The material gives an extensive pattern of sidebands at accessible spinning speeds but has a fairly short proton T_1 and gives excellent signal-to-noise. A typical spectrum of the compound is shown in Figure 1. This was obtained by using a standard 5-mm diameter rotor (Doty Scientific) in a home-built probe of novel design.[19] We employed a flipback pulse sequence,[20] with a Hartmann–Hahn contact time of 8 ms. Power levels during the contact time were 40 and 200 W on the high- (301.42 MHz) and low- (53.86 MHz) frequency channels respectively, giving rise to matched rotating frame frequencies of approximately 110 kHz ($\pi/2$ pulse length 2.3 μs). The spectrum was obtained by signal averaging 512 transients with a recycle delay of 16 s, at a spinning speed of 4.4 kHz. In agreement with the crystal structure but in contrast to Harris, we note a single isotropic resonance from this material (inset to Figure 1). We believe the apparent doubling of resonances noted in the previous NMR work is due to their spectrum being obtained slightly off the magic angle; our line width for this sample (35 Hz, 0.7 ppm) is much less than the separation of the two

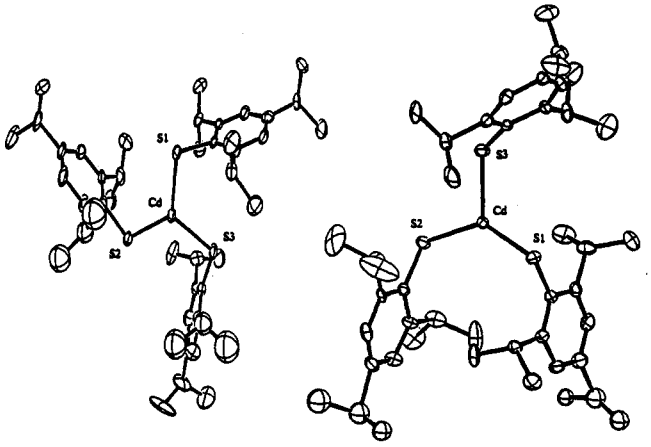

Figure 2. ORTEP diagrams of the anions of $[Ph_4P][Cd(S\text{-}2,4,6\text{-}i\text{-}Pr_3C_6H_2)_3]$ (**1**) and $[(n\text{-}Bu)_4N][Cd(S\text{-}2,4,6\text{-}i\text{-}Pr_3C_6H_2)_3]$ (**2**).

resonances noted by Harris (6 ppm), yet there is no evidence of a splitting of the signal. In earlier off-angle spinning studies of extensive sideband patterns,[21] it was noted that distorted line shapes and apparent splittings could indeed arise. This exemplifies the fact that for large shielding tensors, attention to proper adjustment of the magic angle is of critical importance; where sensitivity permits, we fine adjust the angle on each individual sample.

The chemical shift of mercuric acetate is –2490 ppm with respect to dimethyl mercury. The intensities of the extensive set of rotational sidebands can be used to calculate the principal values of the shielding tensor. However, in order to accurately measure these intensities, it is necessary to tightly control the sample rotation rate, since a variation in spinning speed of $\Delta\nu_R$ will give rise to an excess line width of $N\Delta\nu_R$ in the Nth sideband. If N is large, this will cause significant underestimation of the intensity of the outer sidebands. Even with painstaking control of the spinning speed (our root-mean-square variation in ν_R is approximately 1 Hz), some broadening of the outer sidebands will frequently be noted. To compensate for this, the sideband intensity must be integrated over sufficiently wide limits.

Fitting these sideband intensities to calculated shielding tensors also poses problems. The graphical method of Herzfeld and Berger[22] was aimed primarily at smaller sets of sidebands and cannot directly be applied to tensors whose shielding anisotropy exceeds the spinning speed by a factor greater than 15. The earlier moment analysis of Maricq and Waugh[23] can be directly applied but requires that the intensity of every sideband be accurately measured; furthermore, calculation of the second and particularly the third moment of the sideband pattern puts the greatest statistical weight on the outer sidebands, which are the intensities which, because of spectrometer bandwidth, power rolloff, and spinning speed variation, are the least accurately measurable. The method is thus statistically poor and leads to large errors when used to fit data such as the ones presented here. A naive but surprisingly accurate method exploits the fact that for large tensors, the sideband pattern tends to follow closely the envelope of the static powder pattern, from which the principal values may be obtained by inspection. However, to rigorously fit the tensor, one must do a least-squares fit with a suitable iteration routine to sideband intensities calculated by using the equations derived by Herzfeld and Berger.[22] These calculations are time consuming, since even with Gauss–Legendre quadrature, angular increments of as small as 3° must be used to ensure accuracy in the powder integral. Our procedure has usually been to use the naive inspection method to obtain a good initial guess of the principal values; this estimate is then refined by the least-squares fitting method. We find it statistically superior to fit several sideband patterns simultaneously. By these methods, we estimate our errors in the calculation of large shielding tensors to be 20 ppm or less.

Spectra of other mercury compounds were obtained by using methods similar to those used for mercuric acetate. Spectra of cadmium compounds were obtained at a spectrometer frequency of 66.89 MHz and were referenced to 0.1 M $Cd(ClO_4)$ in H_2O. Most experimental parameters were similar to those used for mercury and have previously been described.[24]

(19) Tang, P.; Chien, W. J.; Harbison, G. S. To be submitted for publication.
(20) Tegenfeldt, J.; Haeberlen, U. *J. Magn. Reson.* **1979**, *36*, 453.
(21) Menger, E. M.; Raleigh, D. P.; Griffin, R. G. *J. Magn. Reson.* **1985**, *63*, 579.
(22) Herzfeld, J.; Berger, A. E. *J. Chem. Phys.* **1980**, *73*, 6021.
(23) Maricq, M. M.; Waugh, J. S. *J. Chem. Phys.* **1979**, *70*, 3300.
(24) Santos, R. A.; Gruff, E. S.; Koch, S. A.; Harbison, G. S. *J. Am. Chem. Soc.* **1990**, *112*, 9257–9263.

Table IV. Metrical Parameters in Three-Coordinate $[M(SR)_3]^{n-}$ Compounds of d^{10} Metals

compound	isomer	S–M–S (deg) (range)	M–S_{av} (Å)	M–S (Å) (range)	ref
$[Ph_4P][Cd(S\text{-}2,4,6\text{-}i\text{-}Pr_3C_6H_2)_3]$ (1)	C_{3h}	122.7 (1)–117.6 (1)	2.420 (4)	2.428 (3)–2.419 (1)	16
$[(n\text{-}Bu)_4N][Cd(S\text{-}2,4,6\text{-}i\text{-}Pr_3C_6H_2)_3]$ (2)	Y	135.3 (1)–100.8 (1)	2.434 (15)	2.455 (4)–2.422 (4)	a
$[(n\text{-}Pr)_4N][Hg(S\text{-}2,4,6\text{-}i\text{-}Pr_3C_6H_2)_3]$ (3)	Y	136.6 (1)–101.3 (1)	2.442 (32)	2.469 (4)–2.397 (4)	16
$[Ph_4P][Hg(S\text{-}2,3,5,6\text{-}Me_4C_6H)_3]$ (5)	Y	134.60 (6)–112.45 (6)	2.432 (44)	2.494 (2)–2.397 (2)	a
$[(n\text{-}Bu)_4N][Hg(SPh)_3]$ (6)	Y	137.1 (1)–102.9 (1)	2.448 (43)	2.507 (3)–2.407 (3)	25
$[Et_4N][Hg(S\text{-}t\text{-}Bu)_3]$	C_{3h}	121.24 (4)–117.90 (4)	2.442 (10)	2.451 (1)–2.436 (1)	30
$[(n\text{-}Pr)_4N][Zn(S\text{-}2,3,5,6\text{-}Me_4C_6H)_3]$	Y	134.10 (8)–110.11 (7)	2.230 (10)	2.243 (2)–2.217 (2)	36
$[Ph_4P]_2[Cu(SPh)_3]$	Y	135.37 (20)–111.7 (2)	2.295 (35)	2.335 (4)–2.274 (4)	35
$[Et_4N]_2[Cu(SPh)_3]$	C_{3h}	121.3 (1)–118.2 (1)	2.250 (9)	2.258 (2)–2.239 (2)	34

[a] This work.

Table V. ^{199}Hg CP/MAS–NMR

compound	geometry	σ_{11}	σ_{22}	σ_{33}	σ_{iso}	$\Delta\sigma$	η
$[Ph_4P][Hg(S\text{-}2,4,6\text{-}i\text{-}Pr_3C_6H_2)_3]$ (4)	C_{3h}	672	−596	−876	−267	1408	0.30
$[(n\text{-}Bu)_4N][Hg(SPh)_3]$ (6)	"Y"	494	−326	−1190	−341	1273	0.97
$[Ph_4P][Hg(S\text{-}2,3,5,6\text{-}Me_4C_6H)_3]$ (5d)	"Y"	685	−275	−1153	−247	1399	0.94
$[Ph_4P][Hg(S\text{-}2,3,5,6\text{-}Me_4C_6H)_3]$ (5u)	"Y"	601	−371	−1057	−276	1315	0.78
$[Hg(S\text{-}2,4,6\text{-}i\text{-}Pr_3C_6H_2)_2]$ (7)	$D_{\infty h}$	627	180	−3852	−1015	4256	0.16
$[Et_4N][Hg(S\text{-}2\text{-}PhC_6H_4)_4]$ (8)	T_d	−379	−429	−491	−433	86.5	0.86

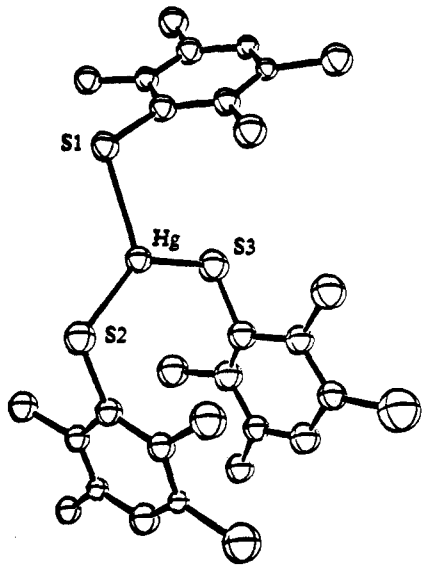

Figure 3. ORTEP diagrams of the anion of $[Ph_4P][Hg(S\text{-}2,3,5,6\text{-}Me_4C_6H)_3]$ (5).

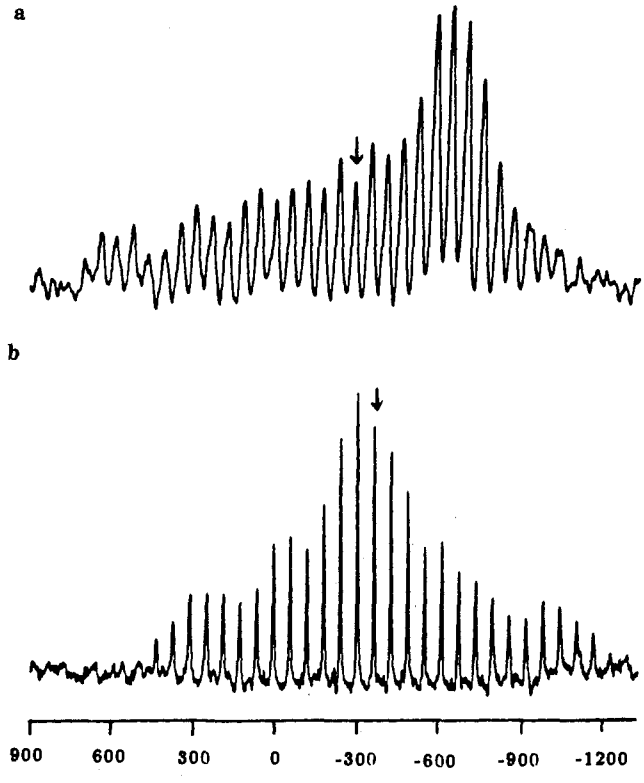

Figure 4. ^{199}Hg CP/MAS–NMR spectra of the trigonal complexes (a) $[Ph_4P][Hg(S\text{-}2,4,6\text{-}i\text{-}Pr_3C_6H_2)_3]$ (4) and (b) $[(n\text{-}Bu)_4N][Hg(SPh)_3]$ (6) both obtained at a rotor spin speed of 3.1 KHz.

Results

X-ray Structures of $[M(SR)_3]^{1-}$ Compounds. We recently reported the synthesis and crystal structure of $[Ph_4P][Cd(S\text{-}2,4,6\text{-}i\text{-}Pr_3C_6H_2)_3]$ (1) (Figure 2).[16] The three-coordinate $[Cd(SR)_3)^{1-}$ anion has an approximate C_{3h} symmetry with each of the three S–Cd–S angles within a few degrees of 120° (Table IV). A change of the cation gave $[(n\text{-}Bu)_4N][Cd(S\text{-}2,4,6\text{-}i\text{-}Pr_3C_6H_2)_3]$ (2), whose crystal structure also reveals a three-coordinate $[Cd(SR)_3]^{1-}$ anion but with a significant distortion from 3-fold symmetry (Figure 2). The S–Cd–S angles show large deviations from 120° (S1–Cd–S2 135.3 (1)°, S1–Cd–S3 123.9°, S2–Cd–S3 100.8 (1)°, but the sum of these angles (360.0°) establishes the CdS_3 unit to be rigorously planar. A rotation of 180° about Cd–S2 bond interchanges this Y-shaped isomer into the C_{3h} (pinwheel) isomer. $[Ph_4P][Hg(S\text{-}2,4,6\text{-}i\text{-}Pr_3C_6H_2)_3]$ (4) is isomorphous with 1. Crystal decay due to the loss of solvent of crystallization precluded a structure determination. It is assumed that 4 is isostructural with 1 and thus has the pinwheel structure. The X-ray structure of $[(n\text{-}Pr)_4N][Hg(S\text{-}2,4,6\text{-}i\text{-}Pr_3C_6H_2)_3]$ (3) revealed the Y-shaped isomer of the $[Hg(SR)_3]^{1-}$ anion.[16] Although 3 is not isomorphous with 2 due to the difference in the cations, the angular distortions of their $[M(S\text{-}2,4,6\text{-}i\text{-}Pr_3C_6H_2)_3]^{1-}$ anions are nearly identical. The structure of $[Ph_4P][Hg(S\text{-}2,3,5,6\text{-}Me_4C_6H)_3]$ (5) was also determined to possess the Y-shaped $[Hg(SR)_3]^{1-}$ isomer (Figure 3). Again, the S–Hg–S angles show distortions from 3-fold symmetry, but the sum of the three angles is 360°. The Hg–S distances in 3 and 5 also show significant distortion; in each compound the Hg–S bond which is opposite the large S–Hg–S angle is ~0.1 Å longer than the other two Hg–S bonds. $[(n\text{-}Bu)_4N][Hg(SPh)_3]$ (6), whose structure was first reported by Christou, shows similar distortions in its Y-shaped $[Hg(SPh)_3]^{1-}$ anion (Table IV).[25]

Solid-State NMR. Figure 4 contrasts the ^{199}Hg CP/MAS spectra of two representative trigonal mercury complexes. Figure 4a shows the spectrum of the complex $[Ph_4P][Hg(S\text{-}2,4,6\text{-}i\text{-}Pr_3C_6H_2)_3]$ (4), which is isostructural with the corresponding

(25) Christou, G.; Folting, K.; Huffman, J. C. *Polyhedron* **1984**, *3*, 1247.

Table VI. ^{113}Pd CP/MAS-NMR

compound	geometry	σ_{11}	σ_{22}	σ_{33}	σ_{iso}	$\Delta\sigma$	η
$[Ph_4P][Cd(S\text{-}2,4,6\text{-}i\text{-}Pr_3C_6H_2)_3]$ (**1**)	C_{3h}	990	545	469	668	483	0.24
$[(n\text{-}Pr)_4N][Cd(S\text{-}2,4,6\text{-}i\text{-}Pr_3C_6H_2)_3$ (**2**)	"Y"	939	540	360	613	489	0.55
$[(n\text{-}Pr)_4N][Cd(S\text{-}2,4,6\text{-}t\text{-}Bu_3C_6H_2)_3]$	"Y"	917	556	369	614	455	0.62

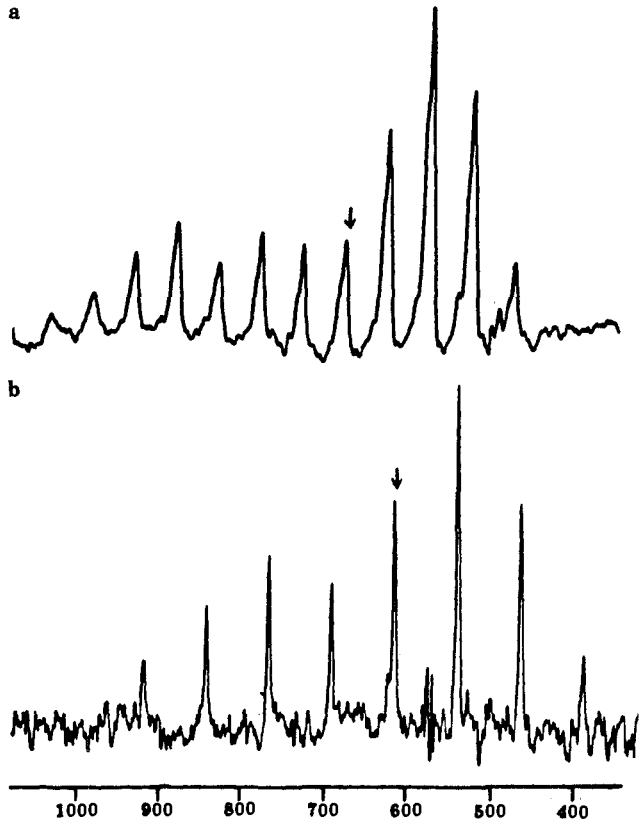

Figure 5. ^{113}Cd CP/MAS-NMR spectra of the trigonal complexes (a) $[Ph_4P][Cd(S\text{-}2,4,6\text{-}i\text{-}Pr_3C_6H_2)_3]$ (**1**) and (b) $[(n\text{-}Bu)_4N][Cd(S\text{-}2,4,6\text{-}i\text{-}Pr_3C_6H_2)_3]$ (**2**) obtained at spin speeds of 3.3 and 4.9 KHz.

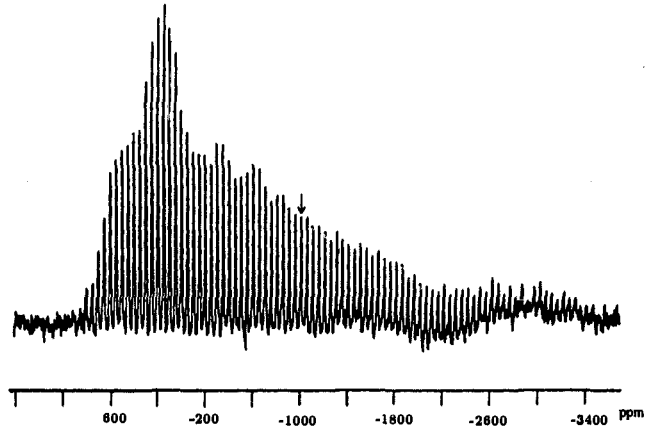

Figure 6. ^{199}Hg CP/MAS-NMR spectrum of the linear complex $[Hg(S\text{-}2,4,6\text{-}i\text{-}Pr_3C_6H_2)_2]$ (**7**) with a spin speed equal to 2.7 KHz.

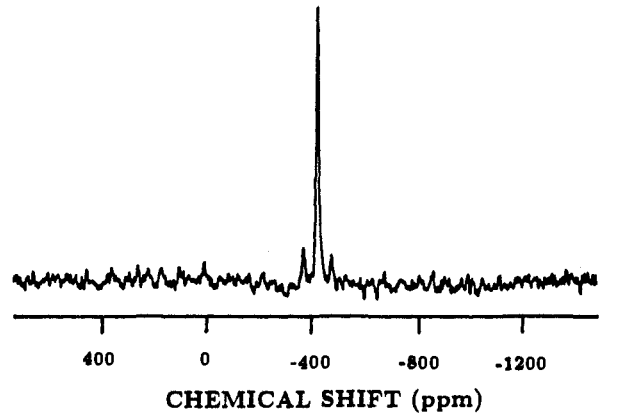

Figure 7. ^{199}Hg CP/MAS-NMR spectrum of $[Et_4N]_2[Hg(S\text{-}2\text{-}PhC_6H_4)_4]$ (**8**), a tetrahedral complex, obtained at a rotor spin speed of 2.8 KHz.

cadmium complex (**1**) and therefore has a pinwheel geometry, with an almost perfect 3-fold axis about the metal. As would be expected for a species with 3-fold rotational symmetry, the sideband pattern traces out the envelope of a shielding tensor with near-axial symmetry. The principal values were obtained by fitting the sideband intensities of several spectra by methods already discussed and are given in Table V. The asymmetry parameter is, as expected, small.

For comparison, in Figure 4b we depict the spectrum of $[(n\text{-}Bu)_4N][Hg(SPh)_3]$ (**6**), which has the Y-shaped structure.[25] The distorted geometry has dramatic effects on the sideband pattern and on the shielding tensor, while the shielding anisotropy is almost unchanged, the asymmetry parameter increases from 0.3 to almost 1.0.

Compound **5**, $[Ph_4P][Hg(S\text{-}2,3,5,6\text{-}Me_4C_6H)_3]$, also crystallizes with a distorted Y-shaped $[HgS_3]$ unit. Two separate crystalline modifications have been detected by CP/MAS, differing by 29 ppm in isotropic shift. It is not clear which modification corresponds with the crystalline form from which the X-ray structure was obtained, but the shielding tensor principal values are very similar to each other and to **6**, again giving an asymmetry parameter of close to 1 in both cases.

In Figure 5 we compare similar trigonal compounds of cadmium. Figure 5a shows the C_{3h} trigonal cadmium derivative $[Ph_4P][Cd(S\text{-}2,4,6\text{-}i\text{-}Pr_3C_6H_2)_3]$ (**1**) isomorphous with **4**; as can be seen from the sideband pattern, its shielding tensor also has a near-axial symmetry. The shielding anisotropy in parts per million is approximately one-third of that of the mercury compound; the asymmetry parameter is nearly identical with **4**. Figure 5b shows the distorted trigonal complex $[(n\text{-}Bu)_4N][Cd(S\text{-}2,4,6\text{-}i\text{-}Pr_3C_6H_2)_3]$ (**2**). The spectrum of a third compound $[(n\text{-}Pr)_4N][Cd(S\text{-}2,4,6\text{-}t\text{-}Bu_3C_6H_2)_3]$ was nearly equivalent to that of **2**. Although its structure was not determined by X-ray crystallography, its anion must crystallize as the Y-shaped isomer. The shielding tensor principal values are summarized in Table VI. A preliminary report of the value for the solid-state chemical shift of $[Ph_4P][Cd(S\text{-}2,4,6\text{-}i\text{-}Pr_3C_6H_2)_3]$ (**1**) was in error.[16]

Figure 6 shows the ^{199}Hg CP/MAS spectrum of the linear mercury thiolate complex $[Hg(S\text{-}2,4,6\text{-}i\text{-}Pr_3C_6H_2)_2]$ (**7**).[16] Because of the enormous shielding anisotropy, the spectrum was taken in two pieces by overlapping CP/MAS spectra. This method was employed earlier for the ^{195}Pt spectrum of K_2PtCl_4.[26] Because of this procedure, the MAS sideband intensities are likely to be somewhat distorted. However, the principal values of the tensor can be obtained with fair accuracy by simple inspection; refinement using only the intensities of the sidebands near the σ_{11} and σ_{22} singularities, which are most strongly dependent on the shielding tensor principal values, with the spectrometer frequency centered 30 kHz downfield of σ_{22} gave the results shown in Table V.

Figure 7 shows the spectrum of a tetrahedral mercury complex, $[Et_4N]_2[Hg(S\text{-}2\text{-}PhC_6H_4)_4]$ (**8**).[27] The $[Hg(SR)_4]^{2-}$ anions of

(26) Sparks, S. W.; Ellis, P. D. *J. Am. Chem. Soc.* **1986**, *108*, 3215.
(27) Silver, A.; Koch, S. A.; Millar, M. To be submitted for publication.

8 have crystallographically imposed S_4 symmetry at the mercury site and should therefore have no shielding anisotropy and no sidebands. The weak sidebands observed may be due to small lattice distortions either caused by stressing the crystals of grinding in preparation for magic angle spinning or by loss of solvent of crystallization.

Discussion

Structures of Hg and Cd Thiolate Compounds. Monomeric Hg(II) thiolate complexes have now been established to possess linear, two-coordinate ($Hg(SR)_2$), three-coordinate ($[Hg(SR)_3]^{1-}$), and four-coordinate ($[Hg(SR)_4]^{2-}$) geometries.[16] It is unusual for a transition metal to form complexes with three different coordination numbers with the same type of ligand.[28] All three of these coordination geometries are likely possibilities for biological Hg–SCys coordination centers. Prior to our work, $[Hg(SR)_4]^{2-}$ and particularly $[Hg(SR)_2]$ complexes were well-precedented, but there was only a single example of a crystallographically characterized $[Hg(SR)_3]^{1-}$ complex.[16,25,29] The X-ray structures of $[Hg(S\text{-}2,4,6\text{-}i\text{-}Pr_3C_6H_2)_3]^{1-}$ and $[Hg(S\text{-}2,3,5,6\text{-}Me_4C_6H)_3]^{1-}$ have provided two additional examples of this coordination geometry. In addition, the recent X-ray structure determination of $[Hg(S\text{-}t\text{-}Bu)_3]^{1-}$ confirmed the three-coordinate structure which had been indicated by vibrational spectroscopy.[30,31] These recent structural results taken with previously reported spectroscopic studies[31-33] indicate that $[Hg(SR)_3]^{1-}$ complexes will be a very common coordination geometry.

The C_{3h} and Y-shaped isomers of $[Cd(S\text{-}2,4,6\text{-}i\text{-}Pr_3C_6H_2)_3]^{1-}$ are the first examples of monomeric, three-coordinate complexes of cadmium with any type of ligand.[16] C_{3h} isomers and Y-shaped isomers have also been observed for $[Cu(SPh)_3]^{2-}$ and $[Zn(SR)_3]^{1-}$ complexes,[34-36] bringing to a total of nine structurally characterized $[M(SR)_3]^{n-}$ complexes for d^{10} metal ions (Table IV). Some general observations can be made concerning the structures of these compounds. The $[MS_3]$ units in both isomers are planar; the sum of the three S–M–S angles in each compound is close to 360°. C_{3h} isomers are characterized by S–M–S angles equal to 120 ± 2° and nearly equal M–S bond distances. The Y-shaped isomers are characterized by a wider range of S–M–S angles and M–S distances within each molecule. In each of the Y isomers, there is one S–M–S angle which is greater than 120°, however, this large angle in each of the six Y-shaped compounds lies in a small range (134–137°). The M–S bond which is opposite to the large angle is longer than the two M–S bonds which make up the large angle. The distortions observed in Y-shaped isomers can be thought of as an intermediate structure along the pathway toward the formation of a linear two-coordinate complex by the dissociation of the third thiolate ligand. The difference between the longest and shortest Hg–S bonds in **3**, **5**, and **6** is 0.07, 0.1, and 0.1 Å, respectively. Although there is only a single example of a Y-shaped $[Cd(SR)_3]^{1-}$ (versus three for $[Hg(SR)_3]^{1-}$), it appears that the distortion in the M–S distances in the CdS_3 unit is smaller than that for $[Hg(SR)_3]^{1-}$ isomers. For Cd and Hg, there is no significant difference in the average M–S distance for the C_{3h} and Y isomers. The long Hg–S bonds and the short Hg–S bonds in the distorted Y-shaped $[Hg(SR)_3]^{1-}$ complexes approach the values observed for Hg–S bonds in $[Hg(SR)_4]^{2-}$ and $[Hg(SR)_2]$ compounds, respectively.[16] However, comparison of averaged Hg–S bonds within a $[Hg(SR)_x]$ coordination unit allows the Hg–S distance to be a good indicator of coordination number.

In general, the coordination chemistry of mercury is significantly different from that of cadmium. In the case of thiolate complexes, the structural chemistry of Cd and Hg are however very similar. The average Cd–S and Hg–S distances in each of the two $[Cd(SR)_3]^{1-}$ structures and the four $[Hg(SR)_3]^{1-}$ structures are nearly equal. Hg–S and Cd–S distances are also equal in $[M(SR)_4]^{2-}$ complexes. Similar metal–ligands distances for analogous compounds with second- and third-row transition metals in the same group is a periodic trend. Linear $[Cd(SR)_2]$ complexes have not been characterized. Although the equilibria between $[M(SR)_2]$, $[M(SR)_3]^{1-}$, and $[M(SR)_4]^{2-}$ compounds appear to favor lower coordination numbers for Hg and higher coordination numbers for Cd, it is anticipated that all three coordination geometry could be important in the biochemistry of both metals.

Solid-State NMR. On examining the shielding tensor data presented here, a clear and consistent, albeit empirical, picture of the behavior of the chemical shielding interaction in linear and trigonal mercury and cadmium complexes emerges. The primary determinant of the tensors, is, as is usually the case, molecular symmetry; species with 3-fold or higher symmetry about a single axis are expected to have axially symmetric shielding tensors, and this should hold for both the symmetric trigonal and linear complexes. The differences between these tensors arise because of the disposition of the metal–sulfur bonds with respect to these symmetry axes. As was pointed out initially by Ellis,[37] sulfur ligands are highly deshielding, and the deshielding effect of these ligands is concentrated in the directions perpendicular to the metal–sulfur vector. For linear mercury complexes, the metal–sulfur axis and asymmetry axis are colinear, meaning that the unique axis of the tensor, along this axis, will be least deshielded and so $\sigma_{zz} < \sigma_{xx} \simeq \sigma_{yy}$.[38] In contrast, in trigonal complexes, the unique axis is perpendicular to the metal sulfur bonds, and so might be expected to be deshielded ($\sigma_{zz} > \sigma_{xx} \simeq \sigma_{yy}$). These predictions are fully borne out by the experimental data. One might also plausibly argue that because the metal–sulfur bonds are colinear in the linear mercury complex, their effects may be expected to be additive resulting in a larger shielding anisotropy than is experienced in the trigonal mercury compounds, where the in-plane deshielding influence of each sulfur will cancel.

What is remarkable is the extent to which the shielding tensors of the trigonal complexes of both mercury and cadmium are sensitive to the in-plane symmetry. For both metals, those complexes with pinwheel symmetry have shielding tensors which are reasonably close to the predicted axial symmetry. However, the relatively small distortion from exact 3-fold symmetry experienced in $[Hg(SR)_3]^{1-}$ compounds **5** and **6** causes the shielding tensor to distort to give an asymmetry parameter of almost 1. One may perhaps rationalize this effect by regarding these complexes as being to some extent intermediate between the symmetric trigonal compounds and the linear complexes—it is notable that the wide sulfur–metal–sulfur angle involves the two most strongly bonded sulfurs in all cases—and so the σ_{22} shielding tensor element is displaced downfield from its usual position in the symmetric trigonal complexes toward the value observed in the linear complexes, while the σ_{33} element is shifted upfield in the distorted complexes, again toward the value it attains in the linear compound. Significantly, the out-of-plane tensor element σ_{11} is entirely unaffected by these in-plane distortions and in fact is very similar in all of the trigonal compounds and in the linear mercury complex. The asymmetry parameter for the Y-shaped $[Cd(S\text{-}2,4,6\text{-}i\text{-}Pr_3C_6H_2)_3]^{1-}$ compound, **2**, is less than that of its Hg analogue, **3**; although the angular distortions in **2** and **3** are nearly identical, the range of M–S bond distances in **2** is less than that in **3**.

(28) Cotton, F. A.; Wilkinson, G. *Advanced Inorganic Chemistry*; John Wiley & Sons: New York, 1988.
(29) Choudhury, S.; Dance, I. G.; Guerney, P. J.; Rae, A. D. *Inorg. Chim. Acta* **1983**, *70*, 227.
(30) Watton, S. P.; Wright, J. G.; MacDonnell, F. M.; Bryson, J. W.; Sabat, M.; O'Halloran, T. V. *J. Am. Chem. Soc.* **1990**, *112*, 2824.
(31) Bowmaker, G. A.; Dance, I. G.; Dobson, B. C.; Rogers, D. A. *Aust. J. Chem.* **1984**, *37*, 1607.
(32) Persson, I.; Zintl, F. *Inorg. Chim. Acta* **1987**, *129*, 47.
(33) Cheesman, B. V.; Arnold, A. P.; Rabenstein, D. L. *J. Am. Chem. Soc.* **1988**, *110*, 6359.
(34) Garner, C. D.; Nicholson, J. R.; Clegg, W. *Inorg. Chem.* **1984**, *23*, 2148.
(35) Coucouvanis, D.; Murphy, C. N.; Kanodia, S. K. *Inorg. Chem.* **1980**, *19*, 2993.
(36) Gruff, E. S.; Koch, S. A. *J. Am. Chem. Soc.* **1989**, *111*, 8762.
(37) Ellis, P. D. *The Multinuclear Approach to NMR Spectroscopy*; Lambert, J. B., Riddell, F. G., Eds.; D. Reidel: The Netherlands, 1983; Chapter 22.
(38) σ_{zz} is, as usual, the element of the traceless anisotropic part of the shielding tensor with the largest absolute magnitude. $\Delta\sigma = |^3/_2\sigma_{zz}|$ while $\eta = (\sigma_{yy} - \sigma_{xx})/\sigma_{zz}$.

Compound **8**, which has exact tetrahedral symmetry about mercury, can be expected to have no shielding anisotropy. However, weak but nonetheless significant rotational sidebands are observed for this species, implying a small but nonzero anisotropic shielding tensor. We speculate that this may be due to distortion of the lattice away from exact symmetry either by strain or by loss of solvent of crystallization. Similar effects have been noted for quadrupolar ions, such as Br^-, in cubic environments,[39] but this is the first time to our knowledge that such effects have been noted for a chemical shielding interaction.

Among the compounds studied, $[Ph_4P][M(S\text{-}2,4,6\text{-}i\text{-}Pr_3C_6H_2)_3]$, **1** and **4**, are especially significant in that they are isomorphous compounds in which only the metal ion has been substituted, and so they allow us to compare the shielding tensors of mercury and cadmium in essentially identical environments. As would be expected, the asymmetry parameters of the two compounds are very similar. The mercury shielding anisotropy exceeds that of the cadmium compound by a factor of 2.92, in line with the general trend that shielding tensors tend to increase in size toward the bottom of the periodic table. We note that a similar ratio of anisotropies has been measured for dimethylmercury and dimethylcadmium with use of liquid crystal solvents.[40] The existence of a fairly consistent trend here is important, since it allows inferences to be drawn about the tensors of species which have as yet not been characterized as model compounds (e.g., linear cadmium thiolates) but might still be conceivable species within proteins.

We note that the shielding tensors obtained by us are quite different from those reported recently by Natan et al. In particular, the shielding anisotropy we obtain for **6** is 30% larger than that obtained earlier for the same compound, with a quite different asymmetry parameter. Significantly, however, the isotropic shift measured by us is very similar to that obtained previously, suggesting that the same compound is indeed being observed. While the fact that Natan et al. did not publish spectra of their trigonal compounds makes it difficult to determine the origin of the discrepancy, we believe it may lie in the method used by them to determine the shielding tensor from their sideband intensities—a moment analysis, which, as already discussed, is highly susceptible to systematic errors. In addition, Natan et al. also measure a shielding anisotropy for the symmetric trigonal complex, $[Hg(S\text{-}t\text{-}Bu)_3]^{1-}$, which is little more than half of that obtained by us for **4**, and a large asymmetry parameter which is quite inconsistent with the near axial symmetry of their material. Finally, the trend observed by them on going from a symmetric to a distorted trigonal complex, in which they observe an increase in the shielding anisotropy but a decrease in the asymmetry parameter, is counterintuitive; in contrast, we observe, in accord with expectations, a large increase in the asymmetry parameter with almost no change in the shielding anisotropy. Therefore, while the isotropic shifts measured by Natan et al. are probably reliable, we believe their shielding tensors are in error.

What, then, are the general prospects for NMR studies of comparable cadmium and mercury species within metal–cysteine proteins? Centers with tetrahedral or near tetrahedral geometry should present no special problems and should be readily observable for both Hg and Cd. The trigonal cadmium complexes have anisotropies somewhat smaller than those previously measured by us for tetrahedral CdS_2N_2 species[24] and should therefore be somewhat more favorable both in solution and the solid state. Proteins of molecular weight of up to 50 kD should be quite manageable in both solution and the solid state, particularly with high speed magic angle spinning systems now becoming widely available. Mercury NMR of proteins is however much more problematic. The 3-fold greater anisotropies will increase solution NMR line widths by a factor of 9 for the trigonal complexes; given the inherently poorer sensitivity of ^{199}Hg relative to ^{113}Cd this may be fatal. The reduction in sensitivity in the solid state will not be so severe; however, signal intensity will be spread over a wide sideband pattern with any MAS system currently available. Strategies for observing in the time domain, where, in contrast to the frequency domain spectrum, the intensity is concentrated into a series of narrow rotational echoes and where the signal-to-noise ratio falls off only as the square root of the shielding anisotropy, may be more favorable, but such techniques are as yet largely unexplored. Nonetheless trigonal mercury compounds are probably observable in smaller proteins, at least by using current spectrometer technology. For the more anisotropic linear mercury thiolates, the picture is more forbidding, since the width of the sideband patterns exceeds the useful bandwidth of most commercial NMR spectrometers (although not ours). In order to have a reasonable expectation of observing a linear mercury species in even a small protein, it is likely that new advances in methodology or instrumentation will be required.

Acknowledgment. This work was supported by NIH Grant GM 31849 to S.K. and GM-39071 to G.H.

Supplementary Material Available: Tables of atomic coordinates, thermal parameters, and bond distances and angles for **2** and **5** and table of atomic coordinates for **3** (23 pages); tables of structure factors for **2** and **5** (34 pages). Ordering information is given on any current masthead page.

(39) Frye, J. S.; Maciel, G. E. *J. Magn. Reson.* **1982**, *48*, 125.
(40) Dalton, J.; Kennedy, J. D.; McFarlane, W.; Wedge, J. R. *Mol. Phys.* **1977**, *34*, 215.